RESEARCH PAPER

Mathematical analysis of oxygen transfer through polydimethylsiloxane membrane between double layers of cell culture channel and gas chamber in microfluidic oxygenator

Min-Cheol Kim · Raymond H. W. Lam · Todd Thorsen · H. Harry Asada

Abstract For successful cell culture in microfluidic devices, precise control of the microenvironment, including gas transfer between the cells and the surrounding medium, is exceptionally important. The work is motivated by a polydimethylsiloxane (PDMS) microfluidic oxygenator chip for mammalian cell culture suggesting that the speed of the oxygen transfer may vary depending on the thickness of a PDMS membrane or the height of a fluid channel. In this paper, a model is presented to describe the oxygen transfer dynamics in the PDMS microfluidic oxygenator chip for mammalian cell culture. Theoretical studies were carried out to evaluate the oxygen profile within the multilayer device, consisting of a gas reservoir, a PDMS membrane, a fluid channel containing growth media, and a cell culture layer. The corresponding semi-analytical solution was derived to evaluate dissolved oxygen concentration within the heterogeneous materials, and was found to be in good agreement with the numerical solution. In addition, a separate analytical solution was obtained to investigate the oxygen pressure drop (OPD) along the cell layer due to oxygen uptake of cells, with experimental validation of the OPD model carried out using human umbilical vein endothelial cells cultured in a PDMS microfluidic oxygenator. Within the theoretical framework, the effects of several microfluidic oxygenator design parameters were studied, including cell type and critical device dimensions.

Min-Cheol Kim and Raymond H. W. Lam are equally contributed to this work.

M.-C. Kim (✉) · R. H. W. Lam · T. Thorsen (✉) ·
H. H. Asada
Department of Mechanical Engineering,
Massachusetts Institute of Technology,
Cambridge, MA 02139, USA
e-mail: mincheol@mit.edu

T. Thorsen
e-mail: thorsen@mit.edu

M.-C. Kim · H. H. Asada
BioSystem and Micromechanics (BioSyM) IRG,
Singapore-MIT Alliance for Research and Technology,
Singapore 117543, Singapore

R. H. W. Lam
Department of Mechanical and Biomedical Engineering,
City University of Hong Kong, Hong Kong, China

1 Introduction

Oxygen transport in biological culture has been essential to many microfluidic applications, including cell-based assays (Brischwein et al. 2003; Tourovskaia et al. 2005; Kane et al. 2006a, b; Wang et al. 2007; Lam et al. 2009; Polinkovsky et al. 2009), bioreactors (Szita et al. 2005; De Bartolo et al. 2006; Sud et al. 2006), and tissue engineering (Radisic et al. 2006a). Tissue engineering often involves moderate/long-term mammalian cell growth within culture platforms or scaffolds to obtain multi-dimensional structures for in vivo implantation (Radisic et al. 2006b; Toh et al. 2007). However, the relatively low solubility of oxygen in aqueous solutions (~ 0.2 mM/atm) is often insufficient to satisfy the demand of dense cell cultures (10^7–10^9 cells/ml) via passive diffusion alone.

Miniaturization of the culture environment combined with an external oxygen supply is an effective approach to increase cell culture oxygenation rates, as diffusion time is proportional to the square of the path length. Researchers

have developed a number of oxygenation techniques for microfluidic devices (Beebe et al. 2002; Leclerc et al. 2004; Zhang et al. 2006; Higgins et al. 2007) which can be mainly categorized as unified and separating types, determined by whether the medium is treated as the oxygen source. For the unified approach, a single culture microchannel is utilized for both oxygenation and nutrient supply, implementing a flowing medium with a defined level of dissolved oxygen (DO) at the channel entry. However, as the cells proliferate, increasing oxygen demands can only be met by increasing the flow rate to levels that potentially introduce unfavorable levels of shear stress on the culture. In contrast, the separating type approach, which has been demonstrated as an effective oxygenation methodology for tissue-scale engineering applications (Radisic et al. 2006b), utilizes devices fabricated in an oxygen-permeable material with the injection of oxygen through distinct microchannels proximal to the culture region. As such, separating type devices create a local constant concentration source of oxygen that rapidly diffuses into the surrounding medium for cellular uptake.

As a structural material of microfluidic devices, polydimethylsiloxane (PDMS) has been recognized as an ideal material for tissue culture due to its gas permeability and excellent molding properties (McDonald et al. 2000). Its high permeability to oxygen ($\sim$620 Barrer for untreated PDMS (Houston et al. 2002); 1 Barrer = 7.5005 $\times$ 10^{-18} m^2 s^{-1} Pa^{-1}) suggests that a separating type oxygenation scheme could be easily implemented via passive diffusion in an ambient environment (Szita et al. 2005; De Bartolo et al. 2006). However, the typical PDMS device thickness ($\sim$5 mm) makes passive oxygenation impractical, with an effective diffusion time (top surface of device to confined microchannels) of $\sim$26 min. Using multilayer soft lithography (Thorsen et al. 2002), the diffusion time can be greatly reduced with an internal membrane oxygenator (Roy et al. 2001) consisting of an overhead control channel containing flowing air or a defined oxygen/nitrogen mixture separated from the flow channel containing cells and culture medium by a thin PDMS membrane of thickness $\sim$10–100 µm that enables rapid gas diffusion (Vollmer et al. 2005). Many separating type microfluidic devices have been recently developed for mammalian and bacterial cell culture, including a PDMS-based chip with a gas perfusion network designed for parallel cell culture (Kane et al. 2006a, b), and oxygenation systems with integrated differential oxygen/nitrogen mixers for long-term cellular growth analysis under differential DO concentrations (Lam et al. 2009; Polinkovsky et al. 2009).

In multilayer separation type microfluidic oxygenators, oxygen molecular transport across the liquid–solid interfaces (i.e., medium-PDMS and medium-cell) can be modeled with two types of boundary conditions: (1) the mass flux of oxygen and (2) continuous oxygen partial pressure (pO$_2$) at the interfaces governed by Henry's law. As a preliminary approximation for the medium-cell interface, it is reasonable to ignore the discrete interfacial oxygen level by assuming that the pO$_2$ and oxygen concentration are both continuous across the interface as most cells contain >70 % of water (Pathi et al. 2005; Radisic et al. 2005; Park et al. 2006; Radisic et al. 2006a). Nevertheless, even when the mass fluxes of oxygen on both material surfaces are identical, with no net oxygen transfer across the interfaces, there is a still an abrupt change in oxygen concentration, especially between medium and PDMS due to the different solubility (or Henry's law coefficients) of the materials (Zanzotto et al. 2002; Patton and Palmer 2006). In solving the oxygen profiles, governing equations for convection–diffusion mass transfer can be converted to differential equations for pO$_2$, which have been previously applied to the analysis of oxygen and nutrient transport between red blood cells and lumen tissue in blood capillaries (Masterton and Hurley 2002).

In this paper, we propose an approximated semi-analytical solution for the general 2-D gas diffusion problem of stacked materials by combining the single layer solutions for materials with individual gas diffusivity and solubility properties using predefined velocity profiles and DO levels. Furthermore, an analytical solution for the estimated oxygen pressure drop (OPD) between the cell monolayer and gas reservoir is derived by taking into consideration of different layers of heterogeneous materials including tissue or cells, culture medium and the PDMS membrane. In particular, this technique is applied to a separating type microfluidic oxygenation device to investigate the performance of oxygen transfer from the gas channel to the cell culture monolayer under different device configurations.

2 Models

2.1 Governing equations of oxygen transfer in microfluidic oxygenator

The mass transfer for a typical microfluidic oxygenator (Zanzotto et al. 2002; Vollmer et al. 2005; Kane et al. 2006a, b; Lam et al. 2009; Polinkovsky et al. 2009) with low microchannel aspect ratios (height/width) can be modeled as a 2-D geometry (Fig. 1), with the double layer channel structure of upper oxygen gas reservoir and lower cell culture chamber separated by a thin oxygen-permeable PDMS membrane. During culture oxygenation, a convective medium flow is imposed from the inlet of cell culture chamber to provide fresh nutrients for the growth of cells located on the lower chamber surface. The governing equations for the transient DO concentrations in cell layer

(c_1), medium (c_2), and PDMS membrane (c_3) are expressed as follows:

$$\frac{\partial c_1(x,y,t)}{\partial t} = D_1 \frac{\partial^2 c_1(x,y,t)}{\partial y^2} - \text{OCR}(x,y,t), \qquad (1)$$
$$\text{for } 0 \leq y \leq H_1$$

$$\frac{\partial c_2(x,y,t)}{\partial t} = D_2 \frac{\partial^2 c_2(x,y,t)}{\partial y^2} - u(y)\frac{\partial c_2(x,y,t)}{\partial x}, \qquad (2)$$
$$\text{for } H_1 \leq y \leq H_1 + H_2$$

$$\frac{\partial c_3(x,y,t)}{\partial t} = D_3 \frac{\partial^2 c_3(x,y,t)}{\partial y^2}, \qquad (3)$$
$$\text{for } H_1 + H_2 \leq y \leq H_1 + H_2 + H_3$$

where H_1 is the cell layer thickness, H_2 is the effective channel height or culture medium layer thickness, H_3 is the PDMS membrane thickness separating the gas and medium channels, t is time, x and y are the horizontal and vertical positions, respectively, and D_i and S_i $(i = 1, 2, 3)$ are the diffusivity and solubility of their corresponding materials (cell, medium, and PDMS, respectively) summarized in Table 1. $\text{OCR}(x, y, t)$ is the oxygen consumption rate of cells based on Michaelis–Menten kinetics (Allen and Bhatia 2003):

$$\text{OCR}(x,y,t) = \frac{V_{\max}\rho_{\text{cell}}c_1(x,y,t)}{K_{\text{m}} + c_1(x,y,t)} \qquad (4)$$

where $V_{\max}$ is the maximum respiration rate per cell [e.g., 4×10^{-17} mol/cell/s for human umbilical vein endothelial cells (HUVEC) and 3.8×10^{-16} mol/cell/s for hepatocyte cells (HC) (Allen and Bhatia 2003)], ρ_{cell} $(=\rho_{\text{cell}}^*/H_1$ [cells/ml]; where ρ_{cell}^* is the surface cell coverage [cells/cm^2]) is the volumetric cell density, and K_{m} $(=S_1 K_{\text{m}}'$; where K_{m}' is Michaelis–Menten constant) is the specific oxygen concentration at which the respiration rate decreases to one half of its maximum value. Depending on cell types, Eq. 4 can have different Michaelis–Menten constants, K_{m}' [e.g., 0.5 mmHg for HUVEC and 5.6 mmHg for HC (Allen and Bhatia 2003)]. In Eqs. 1–3, the diffusive terms along x direction were neglected due to the low aspect ratio of structure (the governing equations still represent most of the channel region where $x \gg H_1 + H_2 + H_3$), while the convective term in Eq. 2 was retained to capture the effect of DO in inlet medium $(c_2(0, y, t) = 0$ [µM], for $H_1 \leq y \leq H_1 + H_2)$. The oxygen concentrations are initially set to be constant over the material domains, i.e., $c_1(x, y, t) = C_1 = 220.25$ [µM], $c_2(x, y, t) = C_2 = 0$ [µM], and $c_3(x, y, t) = C_3 = 249.38$ [µM] at $t = 0$.

The bottom glass substrate is oxygen-impermeable [no mass flux into the bottom glass substrate (Eq. 5)]. On applying Henry's law, pO$_2$ at interfaces between heterogeneous materials should be continuous (Eqs. 6, 8) (Poulsen et al. 2003), while the mass flux of oxygen is balanced

at the interfaces $(y = H_1$ and $H_1 + H_2$ (Eqs. 7, 9)). Hence, the boundary conditions (for $t > 0$) of Eqs. 1–3 are

$$\frac{\partial c_1}{\partial y}(x,y,t) = 0, \quad \text{at } y = 0 \qquad (5)$$

$$\frac{c_1(x,y,t)}{S_1} = \frac{c_2(x,y,t)}{S_2}, \quad \text{at } y = H_1 \qquad (6)$$

$$D_1 \frac{\partial c_1}{\partial y}(x,y,t) = D_2 \frac{\partial c_2}{\partial y}(x,y,t), \quad \text{at } y = H_1 \qquad (7)$$

$$\frac{c_2(x,y,t)}{S_2} = \frac{c_3(x,y,t)}{S_3}, \quad \text{at } y = H_1 + H_2 \qquad (8)$$

$$D_2 \frac{\partial c_2}{\partial y}(x,y,t) = D_3 \frac{\partial c_3}{\partial y}(x,y,t), \quad \text{at } y = H_1 + H_2 \qquad (9)$$

$$c_3(x,y,t) = S_3 p_g, \quad \text{at } y = H_1 + H_2 + H_3. \qquad (10)$$

Under continuous flow of oxygen through the gas channel, the pO$_2$ on the upper surface of the PDMS membrane is modeled as constant (Eq. 10), equal to that of the supplied gas.

2.2 Dimensionless form of the governing equations and boundary conditions

To generalize the problem of oxygen transfer among multiple heterogeneous materials, governing equations and boundary conditions for the transient pO$_2$ (Eqs. 1–10) were converted to the corresponding dimensionless forms (Eqs. 15–23) (Poulsen et al. 2003). The new dimensionless variables g_1, g_2, g_3, m_1, m_2, and m_3 are introduced as

$$g_1(\xi,\psi,\tau) = \frac{P_g}{P_{in}} - \frac{c_1(x,y,t)}{S_1 P_{in}} \qquad (11)$$

$$g_2(\xi,\psi,\tau) = \frac{P_g}{P_{in}} - \frac{c_2(x,y,t)}{S_2 P_{in}} \qquad (12)$$

$$g_3(\xi,\psi,\tau) = \frac{P_g}{P_{in}} - \frac{c_3(x,y,t)}{S_3 P_{in}} \qquad (13)$$

$$m_1(\xi,\psi,\tau) = \frac{\alpha_1^2 Da}{\beta_1} \frac{P_g - g_1 P_{in}}{\bar{K}_{\text{m}} P_{in} + \delta_1(P_g - g_1 P_{in})},$$
$$m_2(\xi,\psi,\tau) = -\frac{Pe\,\gamma_1}{\gamma_2} u^* \frac{\partial g_2}{\partial \xi}, \quad \text{and } m_3(\xi,\psi,\tau) = 0 \quad (14)$$

where ξ $(=x/L)$ and ψ $(=y/H_c)$ are the dimensionless lengths of the x and y coordinates, L and H_c $(=H_1 + H_2)$ are the length and height of medium channel, respectively, τ $(=D_2\,t/H_c^2)$ indicates the dimensionless diffusion time, $P_{in} = 0.001$ atm is the pO$_2$ at the inlet of medium channel, $P_g = 0.1995$ atm (under the supply of air with 5 % CO$_2$) is the pO$_2$ along gas reservoir, Da $(= V_{\max}\rho_{\text{cell}}^* H_c/S_2 P_{in} D_2)$ is the dimensionless Damkohler number which represents the ratio of the overall oxygen uptake rate of cell layer to the diffusive flux of oxygen in medium, $\bar{K}_{\text{m}}(=K_{\text{m}}/S_2 P_{in})$ is

Fig. 1 Schematic of the microchannel used for mass transport modeling, consisting of a gas channel, a PDMS membrane, a medium channel/chamber, a cell layer and an oxygen-impermeable glass substrate
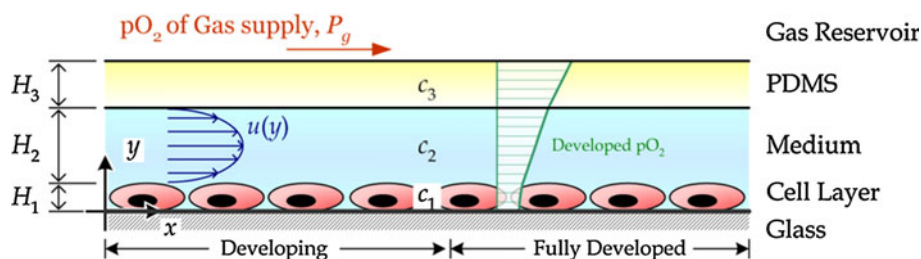

Table 1 Diffusivity and solubility of cells, medium and PDMS

Material	Solubility (mM/atm)	Diffusivity (cm^2/s)
Cell	1.049 (Chakraborty et al. 2007)	9.5×10^{-6} (Chakraborty et al. 2007)
Medium (water)	0.218 at 37 °C (web 1: http://www.engineeringtoolbox.com/oxygen-solubility-water-d_841.html)	2.8×10^{-5} (web 2: http://compost.css.cornell.edu/oxygen/oxygen.diff.water.html)
PDMS	1.25 (Valeur and Brochon 2001; Shiku et al. 2006)	7.88×10^{-5} (Ziomek et al. 1991)[a]

[a] The diffusivity of oxygen in PDMS can vary depending on temperature (Tan et al. 2003; Park et al. 2006)

the dimensionless Michaelis–Menten constant, δ_1 ($=S_1/S_2$) is the ratio of solubility between cell layer and medium, δ_2 ($= S_2/S_3$) is the ratio of solubility between medium and PDMS membrane, Pe ($=UH_2/D_2$) is the Peclet number along medium layer where U is mean velocity in the medium layer, γ_1 ($=H_c/H_2$) is the ratio between medium channel height and effective channel height, γ_2 ($=L/H_c$) is the aspect ratio of culture channel, γ_3 ($=H_3/H_2$) is the thickness ratio between PDMS membrane and medium layer, u^* ($=6U$ $(\beta_2 - \psi)(\psi - \beta_1)$) is the dimensionless fully developed velocity profile in the medium layer with interface boundaries along ψ at β_1 ($=H_1/H_c$) and $\beta_2 = 1$. Substituting the dimensionless parameters into Eqs. 1–3 yield

$$\alpha_1^2 \frac{\partial g_1}{\partial \tau} = \frac{\partial^2 g_1}{\partial \psi^2} + m_1, \quad \text{for } \beta_0 \leq \psi \leq \beta_1 \tag{15}$$

$$\alpha_2^2 \frac{\partial g_2}{\partial \tau} = \frac{\partial^2 g_2}{\partial \psi^2} + m_2, \quad \text{for } \beta_1 \leq \psi \leq \beta_2 \tag{16}$$

$$\alpha_3^2 \frac{\partial g_3}{\partial \tau} = \frac{\partial^2 g_3}{\partial \psi^2} + m_3, \quad \text{for } \beta_2 \leq \psi \leq \beta_3 \tag{17}$$

where $\alpha_1 = \sqrt{D_2/D_1}$, $\alpha_2 = 1$, $\alpha_3 = \sqrt{D_2/D_3}$, $\beta_0 = 0$, and $\beta_3 = (H_1 + H_2 + H_3)/H_c$. The boundary conditions of mass fluxes at the interfaces (Eqs. 5–10) for $\tau > 0$ are converted to the dimensionless form as follows,

$$\frac{\partial g_1}{\partial \psi}(\xi, 0, \tau) = 0 \tag{18}$$

$$g_1(\xi, \beta_1, \tau) = g_2(\xi, \beta_1, \tau) \tag{19}$$

$$\frac{\delta_1}{\alpha_1^2} \frac{\partial g_1}{\partial \psi}(\xi, \beta_1, \tau) = \frac{\partial g_2}{\partial \psi}(\xi, \beta_1, \tau) \tag{20}$$

$$g_2(\xi, \beta_2, \tau) = g_3(\xi, \beta_2, \tau) \tag{21}$$

$$\alpha_3^2 \delta_2 \frac{\partial g_2}{\partial \psi}(\xi, \beta_2, \tau) = \frac{\partial g_3}{\partial \psi}(\xi, \beta_2, \tau) \tag{22}$$

$$g_3(\xi, \beta_3, \tau) = 0 \tag{23}$$

2.3 Semi-analytical solution

The solution of dimensionless oxygen profiles for all material layers (g_i, $i = 1, 2$ and 3) were derived semi-analytically (as described in the Electronic Supplementary Information (ESI)) and coupled with their spatial derivatives, $\partial g_i(\xi, \psi, \tau)/\partial \psi$, at the interfacial boundaries (Mulholland and Cobble 1972; Fredman 2003) (see Eq. S31). The analytical solution for 1-D convection–diffusion problems was extended to 2-D by coupling $g_i(\xi, \psi, \tau)$ in ξ direction and updating the term $\partial g_i/\partial \xi$ in Eq. 16 with the finite difference approximation $\partial g_2(\xi_{j+1}, \psi, \tau_0)/\partial \xi \approx [g_2(\xi_{j+1}, \psi, \tau_0) - g_2(\xi_j, \psi, \tau_0)]/(\xi_{j+1} - \xi_j)$ at the dimensionless priori simulation time (τ_0). Afterward, the dimensionless oxygen profiles, g_i, were converted to the oxygen concentrations of the physical problem, $c_i(x, y, t)$.

The spatial derivative of $g_i(\xi, \psi, \tau)$ can be written as

$$\frac{\partial g_i(\xi, \psi, \tau)}{\partial \psi} = Q_i(\xi, \psi, \Delta\tau)G_i(\xi, \tau) + R_i(\xi, \psi, \Delta\tau)G_{i+1}(\xi, \tau)$$
$$+ P_i(\xi, \psi, \tau_0, \Delta\tau)$$
$$i = 1, 2, 3; 0 \leq \xi \leq 1; \beta_i \leq \psi \leq \beta_{i+1} \tag{24}$$

where $\Delta\tau$ is the dimensionless simulation time step; $P_i(\xi, \psi, \tau_0, \Delta\tau)$, $Q_i(\xi, \psi, \Delta\tau)$ and $R_i(\xi, \psi, \Delta\tau)$ are the coefficients in the linear equation (calculation of the coefficients is described in the ESI); $G_i(\xi, \tau_0)$ and $G_{i+1}(\xi, \tau_0)$ are the boundary values at the bottom and top sides of material i,

respectively, and can be obtained by solving the linear algebra equations in the matrix form $A(\xi)\,X(\xi) = b(\xi)$), which is readily solved line-by-line along the channel axial

(Detailed descriptions of the calculation of $A(\xi)$, $b(\xi)$, $\lambda_{i,n}$, $P_i(\xi, \psi, \tau_0, \Delta\tau)$, $Q_i(\xi, \psi, \Delta\tau)$ and $R_i(\xi, \psi, \Delta\tau)$ are available as ESI.)

$$A(\xi) = \begin{pmatrix} Q_1(\xi,0,\Delta\tau) & R_1(\xi,0,\Delta\tau) & 0 & 0 \\ \frac{\delta_1}{\alpha_1^2}\,Q_1(\xi,\beta_1,\Delta\tau) & \frac{\delta_1}{\alpha_1^2}R_1(\xi,\beta_1,\Delta\tau) - Q_2(\xi,\beta_1,\Delta\tau) & -R_2(\xi,\beta_1,\Delta\tau) & 0 \\ 0 & \alpha_3^2\delta_2 Q_2(\xi,\beta_2,\Delta\tau) & \alpha_3^2\delta_2 R_2(\xi,\beta_2,\Delta\tau) - Q_3(\xi,\beta_2,\Delta\tau) & -R_3(\xi,\beta_2,\Delta\tau) \\ 0 & 0 & 0 & 1 \end{pmatrix}$$

$$b(\xi) = \begin{pmatrix} -P_1(\xi,0,\tau_0,\Delta\tau) \\ -\frac{\delta_1}{\alpha_1^2}P_1(\xi,\beta_1,\tau_0,\Delta\tau) + P_2(\xi,\beta_1,\tau_0,\Delta\tau) \\ -\alpha_3^2\delta_2 P_2(\xi,\beta_2,\tau_0,\Delta\tau) + P_3(\xi,\beta_2,\tau_0,\Delta\tau) \\ 0 \end{pmatrix} \text{ and } X(\xi) = \begin{pmatrix} G_1(\xi,\tau) \\ G_2(\xi,\tau) \\ G_3(\xi,\tau) \\ G_4(\xi,\tau) \end{pmatrix} \tag{25}$$

direction ($0 \le \xi \le 1$) using tri-diagonal matrix algorithm (TDMA) (Conte and deBoor 1972) with Eq. 25.

2.4 Procedures for obtaining semi-analytical

The general procedure for solving the pO$_2$ profile over a stack of different heterogeneous materials in the presence of fully developed fluid flow is summarized as follows:

1. Specify the number of material layers ($N = 3$ in this work), select the final time (t_{final}) and number of time steps (N_{time}) for the calculation of concentration profile over different materials, and calculate the dimensionless final time ($\tau_{final} = t_{final} \times D_2/H_c^2$) and dimensionless time step ($\Delta\tau = \tau_{final}/N_{time}$), and set $\tau_0 = 0$ and $\tau_1 = \tau_0 + \Delta\tau$.
2. Specify the vertical and horizontal grid numbers of each layer depending on the corresponding layer dimensions.
3. Find the eigenvalues spectrum, λ_{in} for $i = 1, 2,\ldots,N$, of each material.
4. Compute $A(\xi)$ and $b(\xi)$ along to the axial direction of channels ($0 \le \xi \le 1$).
5. Set $G_i(\xi, \tau_0) = G_i(\xi, \tau_1)$ for $i = 1, 2,\ldots,N + 1$ and $0 \le \xi \le 1$, and solve the linear matrix equations ($A(\xi)\cdot X(\xi) = b(\xi)$) to update the dimensionless concentration $G_i(\xi, \tau_0)$ at material interfaces. Afterward, substitute $G_i(\xi, \tau_0)$ and $G_i(\xi, \tau_1)$ with updated $P_i(\xi, \psi, \tau_0, \Delta\tau)$, $Q_i(\xi, \psi, \Delta\tau)$ and $R_i(\xi, \psi, \Delta\tau)$ into Eq. 24 to calculate the current spatial distribution of $g_i(\xi, \psi, \tau)$ for $\psi_i \le \psi \le \psi_{i+1}$ and $0 \le \xi \le 1$.
6. If $\tau_1 < \tau_{final}$, set $\tau_0 = \tau_1$ and $\tau_1 = \tau_0 + \Delta\tau$, and go to step 5.
7. Convert $g_i(\xi, \psi, \tau)$ to $c_i(x, y, t)$.

2.5 Oxygen pressure drop along the cell culture monolayer

For high-density of cell cultures at the monolayer, the total oxygen uptake can be significant, inducing a local OPD along the cell culture monolayer. Considering the steady state oxygen transfer in the fully-developed region in an oxygenator described in Fig. 1, the mass fluxes of oxygen across each material layer are identical, as oxygen consumption within the heterogeneous material stack is zero. Such mass fluxes of oxygen can be expressed as

$$q = \frac{D_3 S_3}{H_3}(P_g - P_{2-3}) = \frac{2D_2 S_2}{H_2}(P_{2-3} - P_{2b}) = \frac{2D_2 S_2}{H_2}(P_{2b} - P_{cell}) \tag{26}$$

where P_{2-3} is the pO$_2$ at the interface between PDMS membrane and medium channel, P_{2b} is the bulk pO$_2$ in medium, and P_{cell} is the pO$_2$ along top cell surface. If we correlate q with the cellular oxygen uptake rate at the equilibrium state, q can be written as

$$q = D_1 \frac{\partial c_1}{\partial y}\bigg|_{y=H_{cell}} = \int_0^{H_1} \frac{V_{max}\rho_{cell}c_1}{K_m + c_1}dy \approx \frac{V_{max}\rho_{cell}c_1}{S_1 K'_m + c_1}$$

$$H_1 = \frac{V_{max}\rho_{cell}^* P_{cell}}{K'_m + P_{cell}} \tag{27}$$

where ρ_{cell}^* ($=\rho_{cell} H_1$) is the cell density [cells/cm^2]. In particular, it is assumed that the pO$_2$ in a thin cell layer (~ 5 μm) is uniform along y direction (Cuvelier et al. 2007). Thus, the exact solution for the dimensionless oxygen pressure drop (OPD $= (P_g - P_{cell})/P_g$) between the top cell surface (or cell layer) and gas reservoir can be simplified in following form:

$$\text{OPD} = \frac{P_g - P_{\text{cell}}}{P_g} = \frac{1}{2}(1 + A + B) - \frac{1}{2}\sqrt{(1 - A - B)^2 + 4A}$$

$$A = \frac{K'_m}{P_g} \text{ and } B = \frac{V_{\max}\rho^*_{\text{cell}}}{P_g}\left(\frac{H_3}{D_3 S_3} + \frac{H_2}{D_2 S_2}\right) = \frac{P_{in}Da}{P_g \gamma_1}\left(\alpha_3^2 \delta_2 \gamma_3 + 1\right)$$

$$(28)$$

where the value of A is cell-type specific with a unique Michaelis–Menten constant, while B lumps all of the other general parameters into a single value. The surface plot of OPD (Fig. 2) shows that the gradient of the function OPD with respect to B decreases gradually for $0 \le B \le 1$ as the variable A increases from 0 to 0.03, indicating that the cell type with lower K'_m (~ 0.5 mmHg) will result in a slightly larger OPD than one with higher K'_m (~ 5.6 mmHg) under the equivalent total oxygen uptake rate of cells ($V_{\max}\rho^*_{\text{cell}}$) and identical culture conditions, i.e., environment factors and device configuration.

3 Validation experiment of oxygen pressure drop

3.1 Device design and fabrication

Single layer PDMS ($H_2 = 200$ μm, $H_3 = 5$ mm) devices containing three culture channels described in Fig. 3a, b were fabricated to verify the OPD induced by the oxygen uptake of HUVEC, while the double layer structure of oxygenator was not used because the ~ 100–800 μm membrane thickness (H_3) induced only negligible OPD (data not shown). The PDMS channel was fabricated by pouring 10:1 PDMS monomer/harder mixture on a Si/SU-8 mold, defining the medium channel dimensions. Prior to O_2 plasma bonding to the PDMS substrate, the glass slide
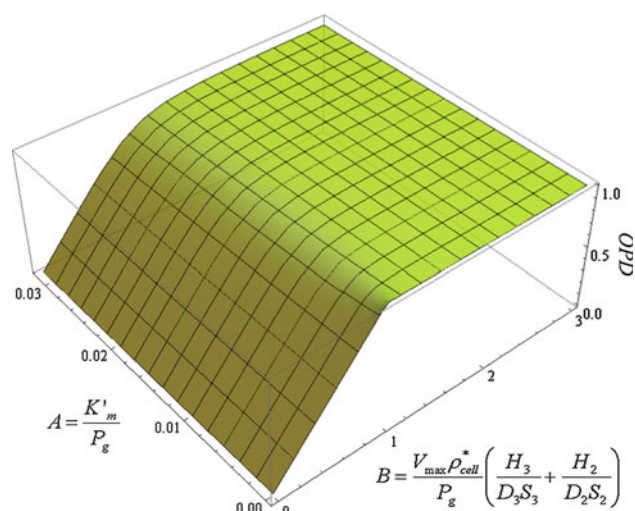

Fig. 2 Surface plot of OPD as a function of variables A and B; it is important to note that the OPD becomes a linear function at the range of B from 0 to 1 and A approaching zero

deposited with oxygen-sensitive platinum (II) octaethyl-porphyrin ketone (PtOEPK)-polystyrene sensors was fabricated as per the diffusion time validation experiment, except that the HF (hydrofluoric acid) etching step was skipped and an extra layer of ~ 8 μm PDMS was spin-coated on a glass deposited with a 4-μm thick sensor layer to create an additional barrier between the cells and the PtOEPK dye, whose cytotoxic effects are unknown. PtOEPK has no oxygen consumption for measurement, so there is still no mass flux of oxygen along the bottom cell surface. The fully developed pO_2 profile along cell, medium, and top PDMS substrate is the same as the model described in Fig. 1.

3.2 Cell culture

HUVECs (Lonza) were cultured in Dulbecco's Modified Eagle Media (DMEM, purchased from Gibco) containing 10 % fetal bovine serum. The cell line was manipulated into a new culture flask pre-coated with 20 mg/ml gelatin (Sigma) in $1 \times$ PBS under sterile tissue culture hoods and cultured in a 5 % CO_2 humidified incubator at 37 °C. Once the cells were confluent, they were trypsinized (0.25 % in EDTA) and passaged at a 1:5 sub-culture ratio.

3.3 Experimental procedures

Each oxygen sensor along the microchannels was calibrated before the microfluidic devices were sterilized by flushing medium channels with 70 % ethanol followed by baking at 80 °C for 2 h. After baking, the fluid channels were rinsed with $1 \times$ phosphate-buffered saline (PBS), with pH 7.4, and degassed by forcing trapped air through the walls of the gas-permeable oxygenator with pressurized PBS buffer. The PDMS surface along flow channels was subsequently pre-coated with fibronectin (Sigma, 0.1 % w/w in $1 \times$ PBS) for 1 h to promote cell attachment. Excess fibronectin was removed by rinsing with $1 \times$ PBS. In preparation for device loading, the cell line was trypsinized, spun down in a centrifuge (1,000 rpm, 5 min), and reconstituted in fresh DMEM at a target cell density. Cells were then seeded into culture channels by a syringe pump (PicoPlus, Harvard Apparatus) at flow rate 0.05 μl/min for 10 min and cultured in a humidified incubator (~ 20 % O_2 and 5 % CO_2 gas supply) without medium flow for 6 h to allow cell spreading and attachment to the treated PDMS surface. After we replaced the channels with fresh media, we performed the DO measurement along the sensor layers without medium flow to record the stabilized sensor readings. Microscopic images were also captured at the sensor regions to determine cell density by counting the cells in the images (Fig. 3c). Each value of OPD, including the results mentioned in the main text, was then calculated

Fig. 3 a Photograph and **b** cross-section schematic diagram of a device for OPD validation. **c** HUVECs were cultured along microchannels with different ρ_{cell}^* to measure the corresponding OPD
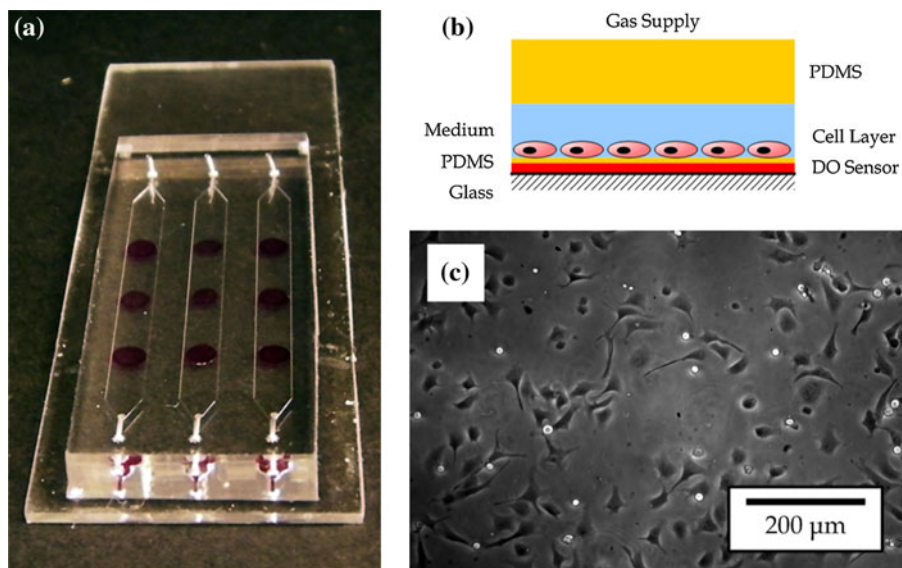
from at least three individual measurements. Another measurement on the chip with 1 cm thick PDMS (H_3) and 200 μm tall channel (H_2), containing $3.08 \pm 0.27 \times 10^4$ cells/cm^2 of HUVEC, also showed a reasonable experimental OPD ($=0.213 \pm$ SD 0.039) with respect to the theoretical value ($=0.2223$) calculated by Eq. 28.

4 Results and discussion

4.1 Comparison of semi-analytical solution with numerical solution

The semi-analytical solution (AS) and the assumption of neglecting the horizontal diffusive effect $\partial^2 c_i/\partial x^2$ ($i = 1, 2, 3$) have been validated by the numerical solution (NS) of the full form of governing equations calculated by a commercial simulation software (COMSOL 3.5, MA). The 2-D model of microfluidic oxygenator consists of three material layers [cell ($H_1 = 5$ μm), medium ($H_2 = 200$ μm) and PDMS ($H_3 = 250$ μm)], with their corresponding diffusivity and solubility values defined in Table 1. A contour plot of the steady state pO$_2$ profile across the layers ($t = 70$ s) in the oxygenator for the pre-defined device dimensions and physical parameters is shown in Fig. 4a (Other sample pO$_2$ profiles are included in the ESI.) The transient variations of pO$_2$ along the top surface of cellular monolayer at five different times (5, 7, 10, 30 and 70 s) shows good agreement between the AS and NS (Fig. 4b).

A sample set of transient dimensionless (g_i) and dimensional (c_i) oxygen concentration profiles (Fig. 4c, d) along the three heterogeneous materials at $x = 3$ mm illustrates the time response of oxygen transfer across

different materials (along y direction) up to the point where the oxygenation profile above the cell culture is fully developed ($t \sim 70$ s). In particular, sharp oxygen concentration jumps are observed at the cell boundary and upper wall of the culture medium filled microchannel (Fig. 4d), due to the lower solubility of oxygen in water (vs. the cells and PDMS).

It is of interest to investigate spatiotemporal variations of the partial pO$_2$ oxygen under different tissue thicknesses of 10, 20, 50, 100 and 150 μm through the AS (Fig. S3). The developing length of pO$_2$ gradually decreases as the cell layer grows in a limited culture channel (constant height: $H_c = H_1 + H_2$), inducing an increasing volumetric ratio of cell layer to medium, because the diffusive resistance of HUVEC (H_1/S_1D_1) is smaller than that of culture medium (H_2/S_2D_2). Furthermore, the AS has an advantage over the NS in that it is possible to more accurately calculate spatial derivatives, $\partial g_i(\xi, \psi, \tau)/\partial\psi$, at the interfacial boundaries (See equations S30 and S31) using the AS once unknown variables of X(ξ) are solved. Thereby, the AS leads to predict dependence of the mass flux of oxygen at the interfacial boundaries on various parameters (Fig. S1–S3).

4.2 Diffusion time of oxygen transfer

The dynamic response of oxygen transfer in an oxygenator was investigated experimentally [detailed experimental method and results were described in the Electronic Supplementary Information (ESI)], in which the mammalian cell layer was replaced by an oxygen-sensitive PtOEPK-polystyrene layer (~ 4 μm). Although the governing equations for the modified oxygenator have no OCR term (due to zero steady state oxygen consumption of sensor

Fig. 4 Comparison between the semi-analytical solution (AS) and the numerical solution (NS) during the development of **a** steady state pO_2 profile ($t = 70$ s) when there is gas transfer through the PDMS membrane and medium flow in the channel. **b** The pO_2 along cell layer at different simulation time indicates reasonable agreement between the AS and the NS. Simulated **c** dimensionless (g_i) and **d** dimensional (c_i) oxygen concentration along y direction at $x = 3$ mm from the channel entrance for $t = 5$, 10, 30 and 70 s
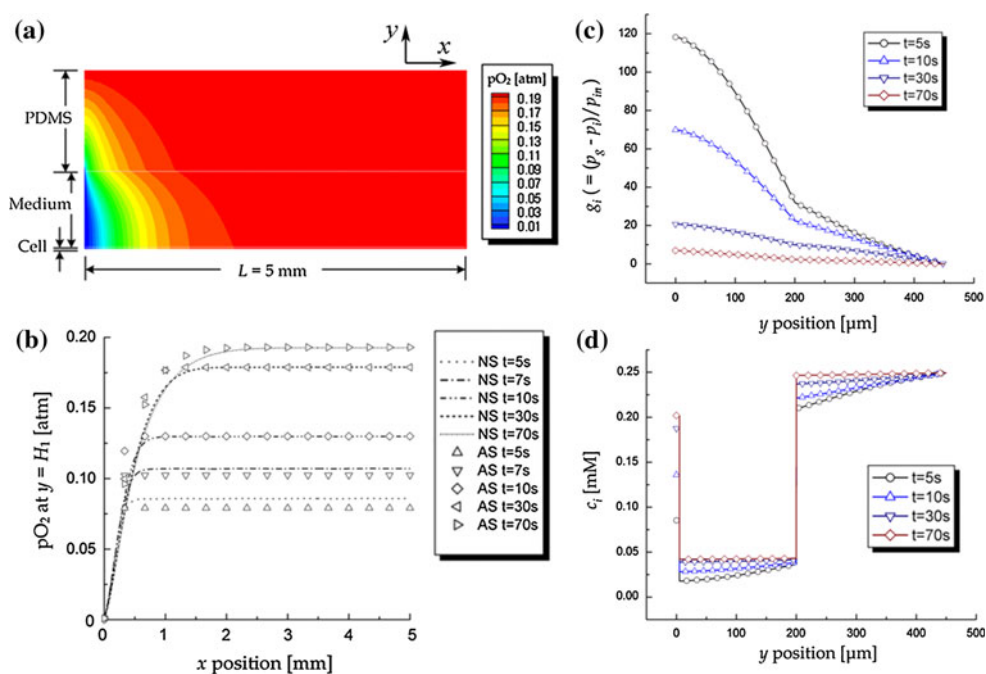
material) and different values of diffusivity ($D_1 = 5.7 \times 10^{-7}$ cm²/s) and solubility ($S_1 = 0.42$ mM/atm) for the base layer, the sensor layer has a negligible effect on the diffusion time (<1.2 % of measured values) because of its thickness ($H_1 \ll H_2$). To investigate the efficiency of oxygenation for the microchannel configuration, the rise time T_r (experimental and simulated), defined by the time required for the sensor pO_2 to reach 90 % of its stabilized value, was plotted against different channel heights and membrane thicknesses (Fig. 5) with reasonable agreement. T_r is largely determined by the medium channel height for a thin PDMS membrane, indicating that T_r is relatively insensitive to the change of H_3 when $H_3 \ll H_2$. On the other hand, when $H_3 \gg H_2$, increment of T_r is proportional to the square of the PDMS membrane thickness, i.e., $T_r \propto H_3^2$. For the typical configuration of single layer microfluidic devices for cell culture applications, the devices are pre-injected with cells along channels and placed in an incubator. In this case, we may consider the PDMS substrate (thickness H_3: ~ 5 mm) as the PDMS membrane of an oxygenator, while the gaseous environment above the PDMS substrate is the gas channel. Considering the device containing microchannel height (H_2) of ~ 100 μm as an example, the rise time (T_r) is then around 3 h which is apparently a significant obstacle to the culture of aerobic cells by passive diffusion.

4.3 Effective channel length

To maintain the long-term growth of cells in microfluidic applications, especially for confluent cell cultures,
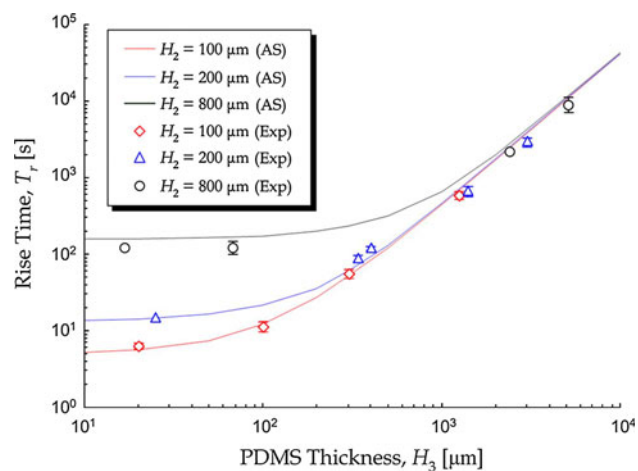

Fig. 5 Semi-analytical solution (AS) and experimental values (Exp) of rise time (T_r) as a function of effective channel height (H_2) and PDMS membrane thickness (H_3). Each data point represents the mean value of at least three independent measurements. The error bars represent the standard deviation of each data point. It should be noted that some error bars are covered by the corresponding data points because the standard deviations are too small

continuous medium flow can be applied along microchannels to maintain the cultivation condition with fresh media such that the waste generated from cells can be removed fast enough. We may perform the oxygenated cell culture by continuously flowing fresh medium into the microfluidic oxygenators, in which the flowing fresh medium continuously oxygenates along the microchannels Therefore, the culture medium from the channel inlet has a characteristic entry length to obtain a fully developed

oxygen concentration profile. The effective channel length L^*, which represents the ratio of oxygen diffusion to convection along the medium channel, can be used to determine whether the bulk of the cell culture chamber region is fully developed ($L^* \gg 1$). In the case where both the cell and PDMS layers are sufficiently thin (H_1/D_1S_1 and $H_3/D_3S_3 \gg H_2/D_2S_2$), we let $L^* = x/PeH_2$ (Vollmer et al. 2005). However, for thick cell and PDMS layers, the variation of pO_2 across the culture medium (along the y axis) is often smaller than the corresponding pO_2 variation in gas layer, especially when PDMS is thick, requiring L^* to be scaled according to the pO_2 in the different material layers. The transition region of oxygen diffusion is assumed to be the position where oxygen starts diffusing to the bottom side of the cell layer with negligible OCR. Thereby, the oxygen partial pressure gradient across the layers may be related to the diffusive resistance, i.e., H_1/D_1S_1, H_2/D_2S_2 and H_3/D_3S_3 for cell, medium, and PDMS layers, respectively. L^* for thick cell and PDMS layers can then be defined as

$$L^* = \frac{x}{PeH_2}\left[\left(\frac{H_1}{D_1S_1} + \frac{H_3}{D_3S_3}\right)\frac{D_2S_2}{H_2} + 1\right]^{-1}. \quad (29)$$

Inspection of the dimensionless channel length (L^*) is very useful in assessing whether a channel region is fully developed with respect to the oxygen concentration gradient. Figure 6 shows the dimensionless pO_2 along cell layer P^*_{cell} [$=(P_{\text{cell}} - P_{\text{in}})/(P_g - P_{\text{in}})$] as a function of L^*, calculated with $Pe = 3$, $Da = 3.93$ (with $\rho^*_{\text{cell}} = 3 \times 10^4$ cells/cm^2), and $K'_m = 0.5$ mmHg for different effective channel heights [$50 < H_2 < 500$ (μm)] (Fig. 6a) and membrane thickness [$50 < H_3 < 5{,}000$ (μm)] (Fig. 6b). It can be observed that the transition region of pO_2 along the cell layer, P^*_{cell}, where the diffusive effect is comparable to the convective one is around $L^* \sim 1$. P^*_{cell} becomes fully developed as $L^* \gg 1$ with a corresponding reduction of OPD, i.e., $P^*_{\text{cell}} \to 1 - \text{OPD}$. In particular, for the case of membrane thickness 5,000 μm shown in Fig. 6b, the P^*_{cell} approaches to a significantly lower level than the other cases as L^* because this case of a thick membrane induces relatively larger OPD ($=0.14$) than all the other cases (OPD < 0.05).

The condition $L^* \gg 1$ may be challenging in some practical implementations with a thick membrane layer in the typical single layer PDMS devices, a significant cell layer thickness in some tissue culture applications ($H_1 > 200$ μm), or a large Peclet number ($Pe \sim 99.2$, culture medium velocity ~ 2.78 mm/s along x direction) for the analysis of cell behaviors under high shear stress (Radisic et al. 2006a). These limitations can be overcome by modifying the oxygenator with extended gas and medium channels prior to the culture chamber to pre-oxygenate the medium.
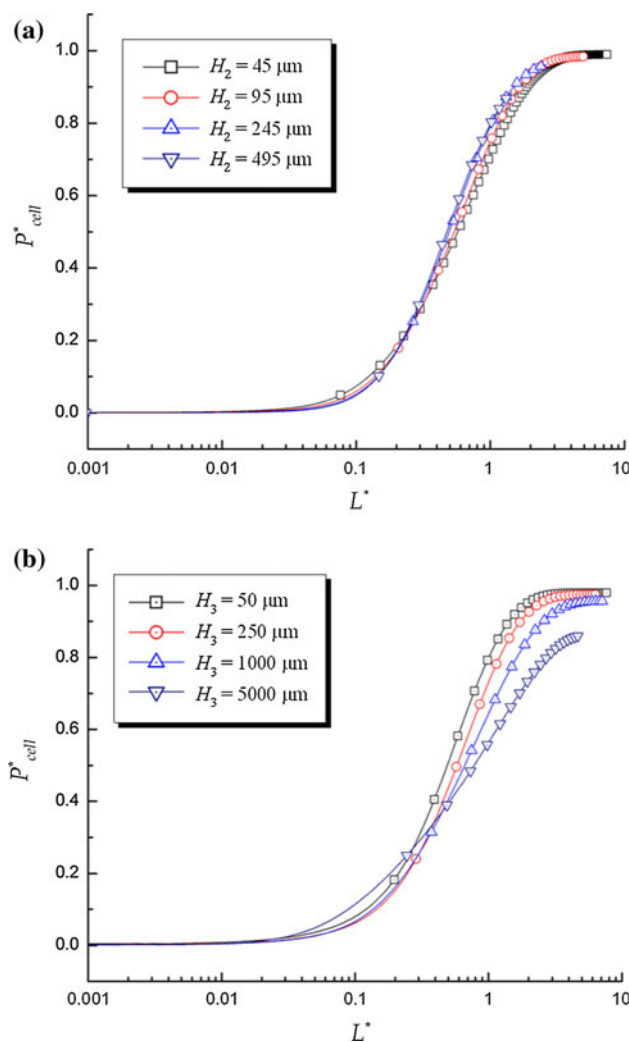

Fig. 6 Plots of P^*_{cell} verses L^* under variations of **a** effective channel height (H_2) and **b** membrane thickness (H_3) representing oxygen diffusion at cell layer ($K'_m = 0.5$ mmHg, $V_{\text{max}} = 4 \times 10^{-17}$ mol/cell/s and $P^*_{\text{cell}} = 3 \times 10^4$ cells/cm^2 for HUVEC) along medium channel with the constant Peclet numbers ($Pe = 6$ in **a** and $Pe = 3$ in **b**)

4.4 Experiment for oxygen pressure drop

Experiments were also performed to verify the OPD of HUVECs along a microchannel (see Fig. 3a) with an equivalent structure for fully developed pO_2 profile described in Fig. 1. HUVECs ($H_1 = 5$ μm) with a surface cell coverage of $\sim 10^3$–10^4 cells/cm^2 were cultured along the microchannel ($H_2 = 200$ μm) constrained by the PDMS microchannel ($H_3 = 5$ mm) with air supplemented with 5 % CO_2 at 37 °C ($pO_2 = 0.1995$ atm). The measured OPD ($0.021 \pm$ SD 0.009, 0.072 ± 0.026, 0.157 ± 0.030, and 0.166 ± 0.033) increases with the surface cell coverage P^*_{cell} [0.67 ± 0.05, 1.54 ± 0.12, 3.68 ± 0.21, and 4.04 ± 0.29 ($\times 10^4$ cells/cm^2), respectively] (see Table 2). This result agrees with the analytical solution in Eq. 28 that

Table 2 Experimental measures of OPD of HUVEC cultured in microchannels

	Total cell coverage($\times 10^4$ cells/cm^2)			
	---	---	---	---
	0.67 ± 0.05 (SD)	1.54 ± 0.12	3.68 ± 0.21	4.04 ± 0.29
OPD	0.021 ± 0.009 (SD)	0.072 ± 0.026	0.157 ± 0.030	0.166 ± 0.033
Equivalent $V_{\max}$ ($\times 10^{-17}$ mol/cell/s)	2.38	3.55	3.23	3.12

OPD is proportional to the surface cell coverage P^*_{cell} for the negligible Michaelis–Menten constant of HUVEC ($K'_{\text{m}} \ll P_g$). Furthermore, the experimental maximum cellular respiration rate $V_{\max}$ ($\sim 3.12 \times 10^{-17}$ mol/cell/s) is of the same order of magnitude as the analytical value in bulk culture environment ($= 4 \times 10^{-17}$ mol/cells/s).

4.5 Insight of oxygen pressure drop

Separating type microfluidic oxygenators should be designed to supply and maintain sufficient oxygen to cells to avoid an anoxic (pO$_2$ $\approx$ 0 mmHg) or hypoxic (pO$_2$ $\approx$ 5–15 mmHg) environments leading to necrosis or stress on aerobic mammalian cells (Roy et al. 2001). However, for cultivation of vascular endothelial cells, maintaining low oxygen level is also important in hypoxia triggers angiogenesis by the induction of vascular endothelial growth factor (VEGF) from tumor cells or fibroblast cells, which leads to angiogenic vessel sprouting formation in the extracelluar matrix (ECM) (Germain et al. 2010). In addition, to maintain an adequate amount of oxygen supply to support confluent cell cultures, the oxygenator should be optimized with respect to the design parameters, including OPD and T_r. Considering the comparatively large oxygen diffusivity and solubility of PDMS listed in Table 1, the membrane thickness should be minimized to enable rapid gas exchange with the cells (or small T_r, as mentioned in the previous section) and small OPD, which includes parameters A (cell-type dependent) and B as a unified value of the device configuration aforementioned in Eq. 28.

The OPD along the cell culture layer for different cell types (HUVEC and HC), surface cell coverage, channel height (H_2), and PDMS thickness (H_3) is plotted in Fig. 7 with $Pe = 3$, based on a fixed medium flow rate. For the case where $A \ll 0.01$ [e.g., HUVEC culture ($K'_{\text{m}} = 0.5$ mmHg) under the supply of air with 5 % CO$_2$ (pO$_2$ = 0.1995 atm)], OPD $\sim B$ when $0 \le B < 1$ and OPD ~ 1 for $B \ge 1$ as shown in Fig. 2. Since B is a linear function of H_2 and H_3 when $B < 1$, B increases linearly with respect to incremental thickness changes in H_2 (Fig. 7a) or H_3 (Fig. 7b) as $A \ll 0.01$, and B is proportional to P^*_{cell} (observed by the change in gradient of OPD for HUVEC). These results imply that cell growth can induce OPD down to hypoxic levels. The population of cells cultured in microchannels may expand and become confluent during long-term cultivation (i.e., large $V_{\max}$); therefore, the oxygen consumption of cells may become noticeably higher than the oxygen supply diffused through the PDMS substrate around the microchannels. In this case, the difference between the uptake rate and oxygen diffusion rate results in high pO$_2$ drop between the cell monolayer and the gas channels. On the other hand, the OPD values are also sensitive to cell type. A comparison between HUVEC (surface coverage $P^*_{\text{cell}} = 3 \times 10^5$ cells/cm^2) and HC ($P^*_{\text{cell}} = 3.16 \times 10^4$ cells/cm^2) with identical B values (equivalent $V_{\max}\rho^*_{\text{cell}}$ and identical device geometry as shown in Fig. 7) indicates that cell types with different K'_m and $V_{\max}$ induce distinct OPD responses, dependent on surface cell coverage ρ^*_{cell}. Both cell type and surface cell coverage constrain the allowable chamber height in a separating type microfluidic oxygenator. In particular, oxygenation with air for 3×10^5 cells/cm^2 of HUVEC requires a cell culture chamber height below ~ 800 μm to avoid generating a hypoxic culture environment as shown in Fig. 7a.

Typical cell culture applications using a single layer of channel structures with a ~ 5-mm thick overhead PDMS substrate are often considered that the gas exchange (e.g., O$_2$ and CO$_2$) is sufficient, yet the corresponding OPD may induce an unfavorable microenvironment for cell growth, as indicated in this study. For instance, the effective diffusion time ($= x^2/2D$) of the typical PDMS device thickness (~ 5 mm) is around 26 min, which means that the diffusion resistance becomes relatively high. In this work, we have investigated that the separating type microfluidic oxygenator can be configured to resolve this constrain of gas transfer. The microfluidic can provide the rapid gas exchange through the overhead PDMS membrane (short stabilizing time), minimize OPD, and locate the fully developed region ($L^* \gg 1$) for the optimal microfluidic cell culture conditions.

A desirable application of gas transport analysis described in this work is the cell cultivation directly on a thin PDMS membrane rather than a gas-impermeable substrate (e.g., glass) underneath cells. Based on Eq. (28), gas exchange of cells is done directly through the PDMS substrate with a great reduction of OPD. In addition, for the hypoxia condition, which has been known as a better
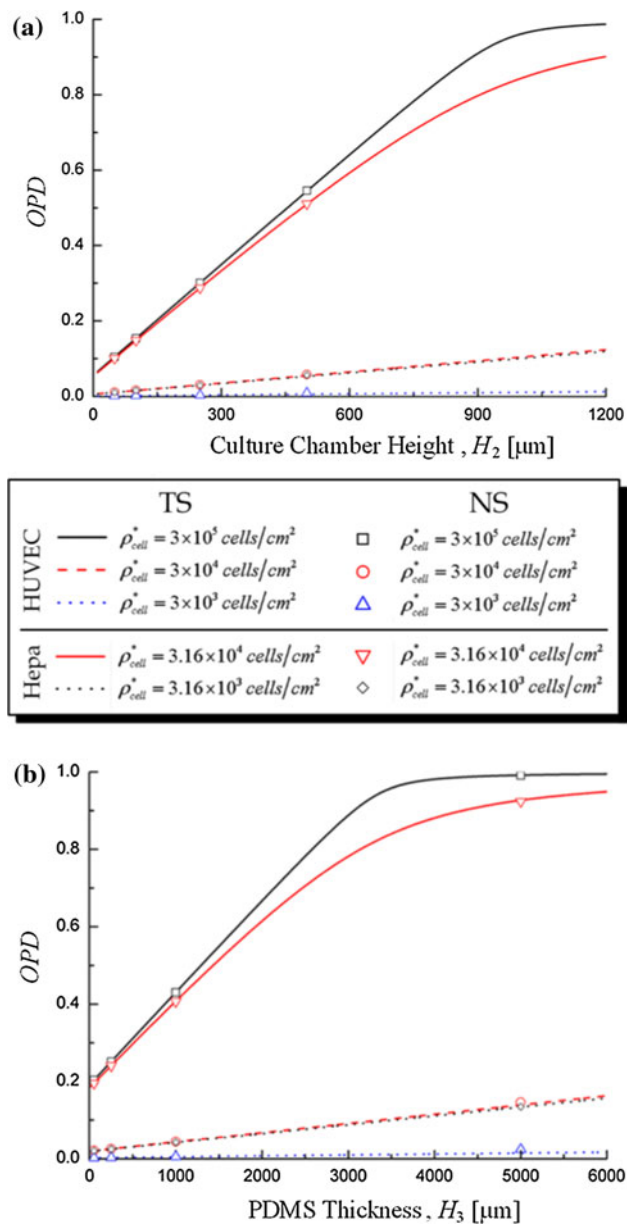
5 Conclusions

The oxygen diffusion process in the typical configuration of separating type microfluidic oxygenator for mammalian cell culture has been investigated through modeling, characterization, and experimental validation. The governing equations underlying dynamics of the 2-D multi-layer mass transfer process have been converted to a general dimensionless form, for which a semi-analytical solution has also been developed by matching the interfacial boundary conditions of 1-D analytical solutions (along y direction) for single layer heterogeneous materials, and numerically approximating over time (t) and channel length (x direction). The design parameters including T_r, OPD, and L^* have been proposed to quantify the oxygenation performance through characterization of the device configuration. The validation of T_r and OPD were performed by experiments. General design considerations for microfluidic oxygenators have also been discussed through the parametric studies, e.g., minimizing chamber and membrane thicknesses for small T_r and OPD, adjusting gas pO_2 levels to compensate a large OPD, and extending the oxygenation channel upstream of the culture region to establish a fully developed oxygen profile ($L^* \gg 1$). This work provides a framework for designing a microfluidic oxygenator, where the miniaturization of such systems for cell physiochemical analysis is of growing interest to the general research community for applications such as drug discovery, personalized medicine and tissue engineering.

Fig. 7 Variation in OPD under two different configurations of **a** channel height and **b** PDMS thickness with two different cell types: HUVEC ($K_m' = 0.5$ mmHg, $V_{max} = 4 \times 10^{-17}$ mol/cell/s and $P_{cell}^* = 3 \times 10^3$, 3×10^4 and 3×10^5 cells/cm^2) and hepatocyte (Hepa) cells ($K_m' = 5.6$ mmHg, $V_{max} = 3.8 \times 10^{-16}$ mol/cell/s and $P_{cell}^* = 3.16 \times 10^3$ and 3.16×10^4 cells/cm^2). All calculated values show excellent agreement between theoretical solution (TS, see Eq. (28)) and numerical solution (NS). Contour plots for these parametric studies (with $P_{cell}^* = 3 \times 10^4$ cells/cm^2 of HUVEC) are available in Figure S1 & S2 in Supplementary Material

condition of angiogenic vessel sprouting in a three-dimensional ECM (Vickerman et al. 2008; Farahat et al. 2012), it can be easily achieved by increasing thickness of the PDMS layer (>5 mm) or channel height based the OPD analysis.

References

Allen JW, Bhatia SN (2003) Formation of steady-state oxygen gradients in vitro—application to liver zonation. Biotechnol Bioeng 82(3):253–262

Beebe DJ, Mensing GA, Walker GM (2002) Physics and applications of microfluidics in biology. Annu Rev Biomed Eng 4:261–286

Brischwein M, Motrescu ER, Cabala R et al (2003) Functional cellular assays with multiparametric silicon sensor chips. Lap Chip 3(4):234–240

Chakraborty S, Balakotaiah V, Bidani A (2007) Multiscale model for pulmonary oxygen uptake and its application to quantify hypoxemia in hepatopulmonary syndrome. J Theor Biol 244(2):190–207

Conte SD, deBoor C (1972) Elementary numerical analysis. McGraw-Hill, New York

Cuvelier D, Thery M, Chu YS et al (2007) The universal dynamics of cell spreading. Curr Biol 17(8):694–699

De Bartolo L, Salerno S, Morelli S et al (2006) Long-term maintenance of human hepatocytes in oxygen-permeable membrane bioreactor. Biomaterials 27(27):4794–4803

Farahat WA, Wood LB, Zervantonakis IK et al (2012) Ensemble analysis of angiogenic growth in three-dimensional microfluidic cell cultures. PLoS ONE 7(5):e37333

Fredman TP (2003) An analytical solution method for composite layer diffusion problems with an application in metallurgy. Heat Mass Transf 39(4):285–295

Germain S, Monnot C, Muller L, Eichmann A (2010) Hypoxia-driven angiogenesis: role of tip cells and extracellular matrix scaffolding. Curr Opin Hematol 17(3):245–251

Higgins JM, Eddington DT, Bhatia SN, Mahadevan L (2007) Sickle cell vasoocclusion and rescue in a microfluidic device. Proc Natl Acad Sci USA 104(51):20496–20500

Houston KS, Weinkauf DH, Stewart FF (2002) Gas transport characteristics of plasma treated poly (dimethylsiloxane) and polyphosphazene membrane materials. J Membr Sci 205(1–2):103–112

Kane BJ, Zinner MJ, Yarmush ML, Toner M (2006a) Liver-specific functional studies in a microfluidic array of primary mammalian hepatocytes. Anal Chem 78(13):4291–4298

Kane BJ, Zinner MJ, Yarmush ML, Toner M (2006b) Liver-specific functional studies in a microfluidic array of primary mammalian hepatocytes. Anal Chem 78(13):4291–4298

Lam RHW, Kim MC, Thorsen T (2009) Culturing aerobic and anaerobic bacteria and mammalian cells with a microfluidic differential oxygenator. Anal Chem 81(14):5918–5924

Leclerc E, Sakai Y, Fujii T (2004) Microfluidic PDMS (poly-dimethylsiloxane) bioreactor for large-scale culture of hepatocytes. Biotechnol Prog 20(3):750–755

Masterton WL, Hurley CN (2002) Chemistry: principles and reactions. Thomson Books/Cole, Belmont

McDonald JC, Duffy DC, Anderson JR et al (2000) Fabrication of microfluidic systems in poly(dimethylsiloxane). Electrophoresis 21(1):27–40

Mulholland GP, Cobble MH (1972) Diffusion through composite media. Int J Heat Mass Transf 15(1):147–160

Park J, Bansal T, Pinelis M, Maharbiz MM (2006) A microsystem for sensing and patterning oxidative microgradients during cell culture. Lab Chip 6(5):611–622

Pathi P, Ma T, Locke BR (2005) Role of nutrient supply on cell growth in bioreactor design for tissue engineering of hematopoietic cells. Biotechnol Bioeng 89(7):743–758

Patton JN, Palmer AF (2006) Numerical simulation of oxygen delivery to muscle tissue in the presence of hemoglobin-based oxygen carriers. Biotechnol Prog 22(4):1025–1049

Polinkovsky M, Gutierrez E, Levchenko A, Groisman A (2009) Fine temporal control of the medium gas content and acidity and on-chip generation of series of oxygen concentrations for cell cultures. Lab Chip 9(8):1073–1084

Poulsen L, Zebger I, Tofte P et al (2003) Oxygen diffusion in bilayer polymer films. J Phys Chem B 107(50):13885–13891

Radisic M, Deen W, Langer R, Vunjak-Novakovic G (2005) Mathematical model of oxygen distribution in engineered cardiac tissue with parallel channel array perfused with culture

medium containing oxygen carriers. Am J Physiol Heart Circ Physiol 288(3):H1278–H1289

Radisic M, Malda J, Epping E, Geng W, Langer R, Vunjak-Novakovic G (2006a) Oxygen gradients correlate with cell density and cell viability in engineered cardiac tissue. Biotechnol Bioeng 93(2):332–343

Radisic M, Park H, Chen F et al (2006b) Biomirnetic approach to cardiac tissue engineering: oxygen carriers and channeled scaffolds. Tissue Eng 12(8):2077–2091

Roy P, Baskaran H, Tilles AW, Yarmush ML, Toner M (2001) Analysis of oxygen transport to hepatocytes in a flat-plate microchannel bioreactor. Ann Biomed Eng 29(11):947–955

Shiku H, Saito T, Wu CC et al (2006) Oxygen permeability of surface-modified poly(dimethylsiloxane) characterized by scanning electrochemical microscopy. Chem Lett 35(2):234–235

Sud D, Mehta G, Mehta K et al (2006) Optical imaging in microfluidic bioreactors enables oxygen monitoring for continuous cell culture. J Biomed Optics 11(5):050504

Szita N, Boccazzi P, Zhang Z et al (2005) Development of a multiplexed microbioreactor system for high-throughput bioprocessing. Lab Chip 5(8):819–826

Tan JL, Tien J, Pirone M, Gray DS et al (2003) Cells lying on a bed of microneedles: an approach to isolate mechanical force. Proc Natl Acad Sci USA 100(4):1484–1489

Thorsen T, Maerkl SJ, Quake SR (2002) Microfluidic large-scale integration. Science 298(5593):580–584

Toh YC, Zhang C, Zhang J et al (2007) A novel 3D mammalian cell perfusion-culture system in microfluidic channels. Lab Chip 7(3):302–309

Tourovskaia A, Figueroa-Masot X, Folch A (2005) Differentiation-on-a-chip: a microfluidic platform for long-term cell culture studies. Lab Chip 5(1):14–19

Valeur B, Brochon JC (2001) New trends in fluorescence spectroscopy: applications to chemical and life. Springer, New York, p 236

Vickerman V, Blundo J, Chung S, Kamm R (2008) Design, fabrication and implementation of a novel multi-parameter control microfluidic platform for three-dimensional cell culture and real-time imaging. Lab Chip 8(9):1468–1477

Vollmer AP, Prostein RF, Gilbert R, Thorsen T (2005) Development of an integrated microfluidic platform for dynamic oxygen sensing and delivery in a flowing medium. Lab Chip 5(10):1059–1066

Wang Z, Kim MC, Marquez M, Thorsen T (2007) High-density microfluidic arrays for cell cytotoxicity analysis. Lab Chip 7(6):740–745

Zanzotto A, Szita N, Schmidt MA, Jensen KF (2002) 2nd annual international IEEE-EMBS special topic conference on micro-technologies in medicine & biology 164–168. Madison, Wisconsin, USA

Zhang ZY, Boccazzi P, Choi HG et al (2006) Microchemostat—microbial continuous culture in a polymer-based, instrumented microbioreactor. Lab Chip 6(7):906–913

Ziomek E, Kirkpatrick N, Reid ID (1991) Effect of poldimethyl siloxane oxygen carriers on the biological bleaching of hardwood kraft pulp by trametes-versicolor. Appl Microbiol Biotechnol 35(5):669–673